



Maps, Colors, and SUVs for Standardized Clinical Reports

Nico Merten^{1,2}, Philipp Genseke³, Bernhard Preim^{1,2}, Michael C. Kreissl^{1,3}, Sylvia Saalfeld^{1,2}

¹Research Campus STIMULATE

²Department of Simulation and Graphics, Otto-von-Guericke University

³Department of Radiology and Nuclear Medicine, University Hospital Magdeburg

To cite this version:

Merten, N., Genseke, P., Preim, B., Kreissl, M. C., Saalfeld, S. Maps, Colors, and SUVs for Standardized Clinical Reports. In Proc. of *18. Jahrestagung der Deutschen Gesellschaft für Computer- und Roboterassistierte Chirurgie (CURAC)*. IN PRINT. Reutlingen, Germany. 2019.

Maps, Colors, and SUVs for Standardized Clinical Reports

Nico Merten^{1,2}, Philipp Genseke³, Bernhard Preim^{1,2}, Michael C. Kreissl^{1,3}, Sylvia Saalfeld^{1,2}

¹ Research Campus *STIMULATE*

² Department of Simulation and Graphics, Otto-von-Guericke University

³ Department of Radiology and Nuclear Medicine, University Hospital Magdeburg
Magdeburg, Germany

Contact: nmerten@isg.cs.uni-magdeburg.de

Abstract

We present a map-based visualization approach of anatomical landmarks and lymph node stations in the thorax. Moreover, a method is presented to create color-codings for such maps. These color-codings are combinations of two categorical color scales for said map elements, and an alternating, sequential color scale for multiple Region of Interest (ROI) segmentations. In clinical practice, nuclear medicine physicians use ROI segmentations to compute Standardized Uptake Values (SUVs), which are important clinical parameters to quantify and compare suspicious findings in PET images, e.g., to assess treatment responses. Therefore, we additionally present a guide to compute reproducible SUVs from PET images and DICOM tag values, since the majority of related work offers theoretical information only.

Keywords: Map-Based Visualizations, Color-Coding, SUV Computation, Clinical Report Generation

1 Problem

In recent years, the (semi-)automatic generation of clinical reports, which can be assessed on screen and paper, has gained increased importance [1, 13]. Two important items in such reports are patient-specific diagnoses and therapy decisions. These are usually discussed and documented during interdisciplinary consultations of clinical experts, such as radiologists, oncologists, surgeons, and nuclear medicine physicians. Such consultations are intrinsically visual, since the aforementioned decisions are derived from assessing medical image data, e.g., PET/CT images. Moreover, using facilities that create documents with a standardized structure and layout benefits the process of mental information retrieval.

However, such reports are usually documents that solely consist of text and tables. On the one hand, this results in documents that reflect cases very objectively, e.g., by listing accurate measurements or by using quasi-standardized phrasing to describe cancerous infiltration of tissue. On the other hand, visualizations can enhance such documents. First, text-only documents do neither reflect the visual nature of the aforementioned decision-making processes, nor are the capabilities of our visual apparatus adequately used, i.e., to conceive images in seconds [15]. Secondly, since reporting is a combined effort of various authors, for each part, the degrees of quality and detail can vary, which in turn may hinder reproducible interpretations of findings or decisions [11]. Finally, although clinical experts are well-trained to extract crucial pieces of information out of large texts, this process is prone to errors, because decision-altering details can remain occult to readers.

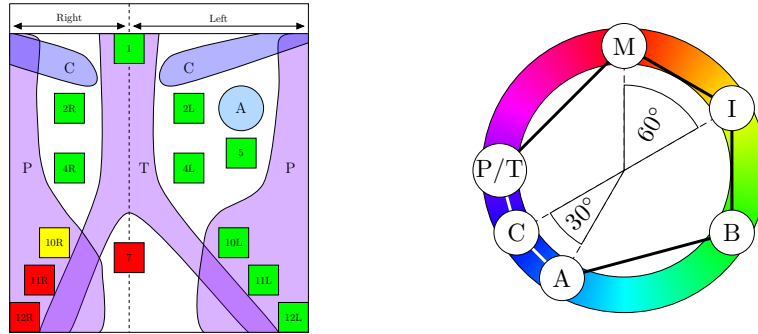


Fig. 1: The proposed map visualizations of LNS staging diagnoses and anatomical landmarks (left) and their default color-coding (right). The color wheel represents the HSV color model. The colors are plotted in clockwise direction, with **Malign** at red (0/360° for H), **Inconclusive** at yellow (60°), and **Benign** at green (120°). The asymmetrical map layout represents the unequal primary bronchi lengths between the **Trachea** and **Parenchyma**, and to avoid visual clutter due to the **Aorta** and **LNS 5**. At the top, the **Claviculae** separate **LNS 1** from **2R/L**.

A map-based visualization approach is presented to enhance reports by stylized depictions, which is inspired by other map-based visualizations in clinical workflows, e. g., Bull’s Eye Plots to diagnose myocardial perfusion defects [6, 7]. Here, maps depict anatomical landmarks and *Lymph Node Stations* (LNSs) in the thorax. These landmarks are simplified frontal cross-sections of the aorta, trachea, clavicle bones and lung parenchyma, while the LNSs are anatomical regions that group multiple nearby lymph nodes [9]. The two main contributions of this work are two color-coding methods and a guide to compute SUVs from PET image values, e. g., from *Region Of Interest* (ROI) segmentations. Selecting *appropriate* color-codings is an important aspect for map and medical image visualizations [2]. Thus, methods are presented that generate color-codings for the aforementioned map elements and ROIs using the HSV color model. Moreover, a guide is presented to compute reproducible *Standardized Uptake Values* (SUVs). There exists related work that describes the computation of SUVs, but in most cases this process is described in theory only [3]. If more practical descriptions are provided, the lack of specific input and output values makes it challenging to reproduce results.

2 Material and Methods

In this section, the color-coding methods and SUV computation guide are presented. Both contributions are extensions of a larger, semi-automatic processing pipeline for clinical reports (cf. Fig. 3), which is implemented in MeVisLab 2.8.2 [8, 12].

2.1 Color-Coding – Lymph Node Stations and Anatomical Landmarks

The proposed approach requires a color-coding for three LNS staging diagnoses, namely benign, malign and inconclusive, and four anatomical landmarks, namely the aorta, lung parenchyma, clavicle bones, and trachea. These landmarks provide spatial references for the LNS [9]. For simplification, the same hue is assigned to the trachea and parenchyma landmarks, since they belong to the same organ.

This results in six map elements that can be regarded as nominal data. Nominal data is usually color-coded via categorical color scales, which introduce large hue differences to generate color palettes [2]. In Figure 1, the default color-coding is depicted in the HSV color wheel, with the hue axis plotted in clockwise direction. For example, Malign marks red (0/360°) and Benign marks green (120°). Since it is important to visually distinguish the individual LNS staging diagnoses, they are placed in 60°steps from each other. This guarantees that they are placed in different, major color zones. In the default case, the three diagnostic categories are placed on red, yellow and green, which results in the easy-to-understand *traffic light color-coding*. In contrast, landmark hues are placed in 30°steps from each other with the pivotal landmark hue (here: Clavicularae) being defined as the complementary color of the pivotal LNS staging hue (here: Inconclusive). On the one hand, this makes resulting landmark colors more similar, but still easy to distinguish. On the other hand, for the default version, this results in landmark colors having blue-like tones, which draw minimal visual attention. This hue placement is an adaption of the harmonic *Y-Type* template by Itten [4], which creates two non-overlapping, complementary color groups.

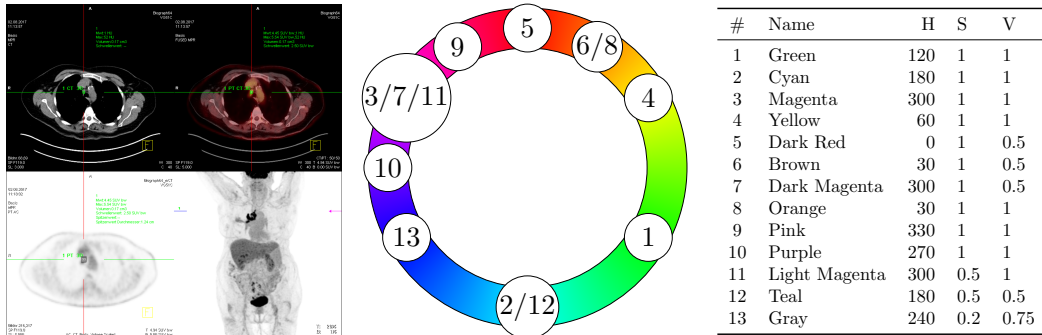


Fig. 2: **Left:** An exported screenshot of the VG51C toolbox with a ROI around LNS 10R. **Middle/Right:** The first thirteen ROI colors in the toolbox depicted in a HSV color wheel and listed in a table. For simplification purposes, only the hues are depicted. While many colors are defined in some sections, e. g., around magenta (300° for H), some areas are barely used, e. g., around green (120° for H). Given the irregular color placement, it appears that the used color palette is hard-coded.

Table 1: *Solutions for Eq. 1 and resulting hues for $N = 9$ with respect to the default color hexagon from Figure 1.*

B_H	R_H	Hue for i -th Color via $(ROIC_i)_H$								
		1	2	3	4	5	6	7	8	9
120	240	144	216	288	168	240	312	192	264	336

Assuming that the saturation and value components of all colors equal 1.0, from a geometrical point of view, this results in an irregular, convex hexagon. Color changes can be geometrically interpreted as rotations (hue), scaling (saturation), or vertical translations (value) of the hexagon inside the HSV color model cylinder. When using the aforementioned report generation software, users can adapt the color-coding interactively by changing the hue, saturation, or value parameters of one color and, consequently, all colors are updated.

2.2 Color-Coding – Adding Region of Interest Colors

In addition to color-coding LNSs and landmarks, ROI segmentation masks can also be color-coded. Existing clinical software toolboxes, e. g., *Siemens Syngo VG51C* (Siemens Healthcare, Erlangen, Germany; VG51C), offer ROI segmentation, SUV computation, and image-based export functionalities that can be combined and used for reports. In clinical practice, ROI segmentation tools are used to mask suspicious image regions and after ROI definition, medical images are superimposed by color-coded outlines or areas. For example, in ^{18}F -FDG PET scans, suspicious hotspots are encompassed and assessed, since they can point to cancerous tissue.

The first thirteen ROI colors of the VG51C toolbox are shown in Figure 2. While some hue sections are barely used, e. g., around green, some areas are cluttered, e. g., around orange and magenta. The latter results in a shortcoming, since the depicted color palette is used for ROIs that superimpose color-coded PET images. In the VG51C software, a black-red-orange-yellow-white color scale is used for PET images, which, in combination with the ROI color-coding, can result in ambiguous color information on screen and paper. Consequently, this can hinder reproducibility of ROI segmentations via reports. To overcome this, the VG51C software offers additional gray scale views of PET and CT slices that have a high contrast to ROI boundary colors (cf. Fig. 2).

In the following, a color-coding method for ROI segmentations is presented that overcomes the aforementioned shortcoming. For simplification purposes, the default color-coding from Figure 1 will be assumed, e. g., with the saturation and value of all ROI colors equal 1.0. However, when LNS and landmark colors are adapted, ROIs color-codings are affected similarly, i. e., moving them through the HSV model cylinder. This is a useful feature, since the aforementioned PET image color-coding is manufacturer-dependent, which makes the proposed methods feasible for various clinical software toolboxes. The proposed method is expressed by two equations, which require the number of ROIs (N), the *type* of N , $t(N)$, and the hue range R_H in which ROIs are defined. R_H is defined by $R_H := 360 - \min(B_H M_H)$, which is the minimum distance between the **M**align and **B**enign hues (cf. Fig. 1). The first equation is given by

$$(ROIC_i)_H = B_H + \left(\frac{R_H}{(N+1)} \times \text{step}_{t(N)}(C_i) \right), \quad \forall i \in [1, N] \quad (1)$$

which defines a hue for the i -th ROI for N -many colors. The second equation, namely $\text{step}(C_i)$, depends on $t(N)$ and assigns different hues to subsequently defined ROIs, e. g., between the 2nd and 3rd ROI color. N can be one of four types and, consequently, a different step equation is used: $t(N)$ can be even ($\text{step}_e(C_i)$), odd and not prime ($\text{step}_o(C_i)$), or prime with an even (e. g., 5, $\text{step}_{pe}(C_i)$) or odd (e. g., 7, $\text{step}_{po}(C_i)$) number of elements to the left and right of the pivotal element, e. g., 4 for $N = 7$. In the following, the four step equations are listed:

$$\begin{aligned} \text{step}_e(C_i) &= \left(1 + \sum_{j=1}^{C_i-1} \begin{cases} 4, & \text{if } i = \frac{N}{2} \\ 2, & \text{otherwise} \end{cases} \right) \% (N+1) & \text{step}_o(C_i) &= \left(1 + \sum_{j=1}^{C_i-1} \begin{cases} \max PF(N) + 2 & \text{if } i \% \left(\frac{N}{\max PF(N)} \right) = 0 \\ \max PF(N) & \text{otherwise} \end{cases} \right) \% (N+1) \\ \text{step}_{pe}(C_i) &= \left(1 + \sum_{j=1}^{C_i-1} \begin{cases} \frac{N+1}{2} + 2, & \text{if } i \text{ is Even}(i) \wedge i < \frac{N-1}{2} \\ \frac{N-1}{4} + 1, & \text{if } i = \frac{N-1}{2} \\ \frac{N-1}{4}, & \text{if } i = \frac{N+1}{2} \\ \frac{N+1}{2} + 2, & \text{if } i = \frac{N+1}{2} \\ \frac{N+1}{2} + 2, & \text{if } i \text{ is Odd}(i) \wedge i > \frac{N+1}{2} \\ \frac{N-1}{2} + 2, & \text{otherwise} \end{cases} \right) \% (N+1) & \text{step}_{po}(C_i) &= \left(1 + \sum_{j=1}^{C_i-1} \begin{cases} \frac{N+1}{2} + 2, & \text{if } i \text{ is Even}(i) \wedge i < \frac{N-1}{2} \\ \frac{3N-1}{4}, & \text{if } i = \frac{N-1}{2} \\ \frac{3(N+1)}{4}, & \text{if } i = \frac{N+1}{2} \\ \frac{N+1}{2} + 2, & \text{if } i \text{ is Odd}(i) \wedge i > \frac{N+1}{2} \\ \frac{N-1}{2} + 2, & \text{otherwise} \end{cases} \right) \% (N+1) \end{aligned}$$

For each color C_i , the equations return a factor that donates the hue of $ROIC_i$ relative to B_H . The function $\max PF(N)$ in $\text{step}_o(C_i)$ returns the maximum of the prime factorization of N , e. g., 5 for $N = 15$. In Table 1, results using $\text{step}_o(C_i)$ and $N = 9$ are listed, while the resulting color palette is depicted in Figure 3.

2.3 SUV Computation

SUVs are computed by combining PET image and DICOM tag values, i.e., patient data and information about the administered radiopharmaceutical and, subsequently, they are used for diagnoses and therapy decisions. Generally, they describe how much of an administered radiopharmaceutical is absorbed by the patient's anatomy. This provides an indication of how metabolically active anatomical regions are, while suspiciously high uptakes can point to cancerous or metastatic tissue. There exists related work that describes the computation of SUVs, but in most cases the computation process is only described from a theoretical point of view [3]. Moreover, if more descriptions are presented, no further information about specific input and output values is provided, which makes it challenging to reproduce results [14]. Therefore, the method in Algorithm 1 below describes how PET image values are converted into SUV_{BW} values, which are SUVs normalized with the patient's bodyweight. In clinical toolboxes, SUVs are usually computed for the single *hottest* voxel value (SUV_{max}) or the average of all ROI-masked PET image values (SUV_{μ}). However, Algorithm 1 can be applied to any PET image value. There exist various types of SUVs, but this work is focused on the computation of SUV_{BW} values, since they are used in the VG51C software and allow for an evaluation regarding computation accuracy.

3 Results

The results are depicted in Figure 3. On the left, an exemplary report is presented, which is divided into four parts. At the top, information about the hospital and responsible physicians are compiled. In the second part, patient-specific data, an N-staging suggestion, and a therapy decision is listed. Furthermore, a color-coding legend is shown that can be used to interpret the 2D map on the right with LNS diagnoses (cf. Fig. 1). The suggested N-staging is derived from the LNS diagnoses and represents the N-component of the *Tumor, Node, and Metastasis* (TNM) staging system that describes suspicious findings in nearby lymph nodes [10]. In the third part, a frontal PET *Maximum Intensity Projection* (MIP) image with color-coded ROIs is shown and the table next to it lists additional information for each ROI, namely a user-defined name, its color, the corresponding PET slice, and its volume. Moreover, the table also lists PET quantification data for all ROIs, namely their respective $Count_{max}$, which is the highest PET image value, the resulting $SUV_{max;BW}$ value, which was obtained with Algorithm 1, and a $SUV_{\mu;BW}$ value, which is the average SUV_{BW} inside each ROI. The color wheels on the right depict ROI color-codings for varying N using the respective step equation. Since nine ROIs were defined for the depicted report, the upmost color wheel was used for color-coding. In the last part, acquisition- and SUV computation-related data is listed, which is intended to create a strong connection between the underlying image data, the ROI segmentations and SUV computations, and the diagnosis and therapy decisions derived thereof.

4 Discussion

When comparing the baseline color-coding from the VG51C toolbox with the proposed method (cf. Figs. 2 and 3), the proposed method does not define colors in the hue range of color-coded PET images, which minimizes the risk of misinterpretations. However, this only applies if the default traffic light color-coding is used. Moreover,

```
# Load PET Data Set
PETdataSet = dicomRead(fileOnHardDrive)
# Get PET Image Value
PETimageValue = PETdataSet.getVoxelValue(x, y, z)
# Get DICOM Tags (expected units are shown in square brackets, e.g. [s] for seconds)
radioStartTime = PETdataSet.getTagValue([0x0018, 0x1072]) # [hhmmss]
radioTotalDose = PETdataSet.getTagValue([0x0018, 0x1074]) # [Bq]
radioHalfLife = PETdataSet.getTagValue([0x0018, 0x1075]) # [s]
acquisitionDate = PETdataSet.getTagValue([0x0008, 0x0022]) # [yyyymmdd]
acquisitionTime = PETdataSet.getTagValue([0x0008, 0x0032]) # [hhmmss]
seriesDate = PETdataSet.getTagValue([0x0008, 0x0021]) # [yyyymmdd]
seriesTime = PETdataSet.getTagValue([0x0008, 0x0031]) # [hhmmss]
patientWeight = PETdataSet.getTagValue([0x0010, 0x1030]) # [Kg]
rescaleIntercept = PETdataSet.getTagValue([0x0028, 0x1052]) # [scalar]
rescaleSlope = PETdataSet.getTagValue([0x0028, 0x1053]) # [scalar]
# Compute SUV
administrationDateTime = seriesDate + "." + radioStartTime # [yyyymmdd.hhmmss]
seriesDateTime = seriesDate + "." + seriesTime # [yyyymmdd.hhmmss]
radioDecayTime = seriesDateTime - administrationDateTime # [s]
radioDecayDose = radioTotalDose * exp(-radioDecayTime * (log(2)/radioHalfLife)) # [Bq]
BWscaleFactor = (patientWeight * 1000) / decayedDose # [g/Bq]
SUVbw = (PETimageValue + rescaleIntercept) * rescaleSlope * BWscaleFactor
```

Alg. 1: SUV_{BW} Computation via DICOM tag values.

the proposed palettes are not hard-coded and depend on the number of defined ROIs. If implemented, the current palette should not be updated with each new ROI, i. e., updating the color-coding repeatedly. Practically, a fixed color palette size should be defined by default and adapted during report generation and export.

The proposed color-coding methods use the HSV color space. It can be argued that this color space represents a fair tradeoff between usability for non-visualization domain experts and perceived color differences between ROI colors. On the one hand, for subsequently defined ROIs, the step equations guarantee a large hue difference, which makes the colors easy to distinguish, even if they are defined in the same image. Since the proposed equations define ROI colors with respect to B_H , the first ROI colors are defined near B_H and the color palette will slowly converge towards M_H . When using software tools to define ROIs, clinical experts encompass suspicious image regions, i. e., regions that will most likely be diagnosed to be inconclusive or malign. This lowers the risk of mentally connecting ROI color-codings with image regions diagnosed as malign, which could alter diagnoses and therapy decisions. On the other hand, equidistantly defined colors in HSV color space do not result in equidistantly perceived color differences. Using perceptually uniform color spaces, e. g., CIELAB, could result in better results, but using them as GUI widgets, e. g., the CIELAB *shoe sole*, would be less beneficial for clinical toolkits than a simple color wheel. Furthermore, in contrast to the VG51C color palette, the proposed methods only alter hue values and keep the saturation and value components constant (cf. Fig. 1 and 2). This limits the proposed methods, since varying saturations and values could also offer better results, but it is challenging to perceive ROIs colors with low saturation and value components due to grayscale MIPs of PET images. Practically, the definition of color palettes should generally be done in the background and only brought to the users' attention if specifically queried, e. g., to define special color palettes in the case of color vision deficiencies.

Case Report – (Mrs.) Doe, Jane

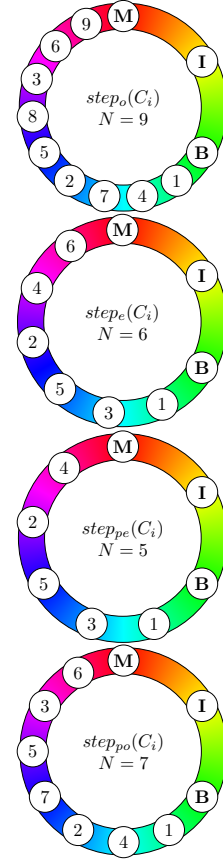
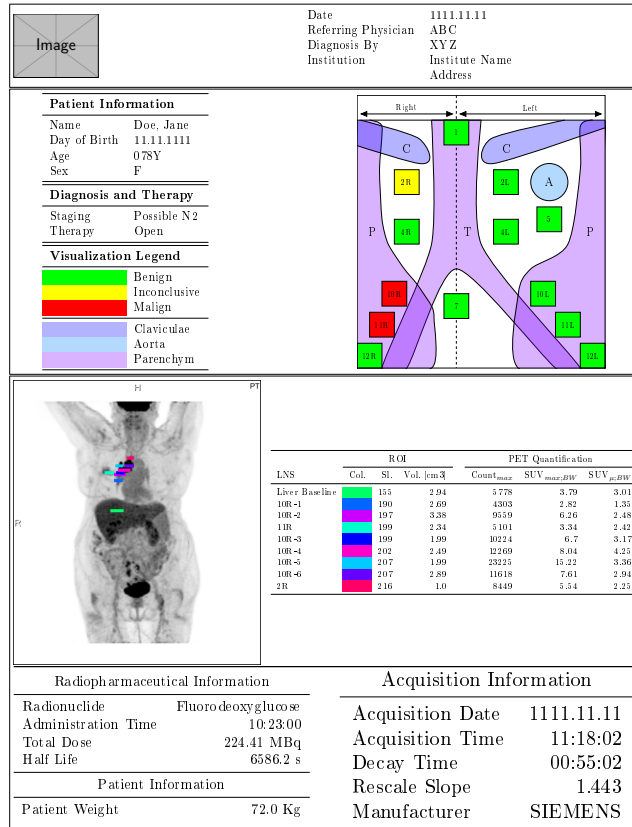


Fig. 3: On the left, an exemplary report with a color-coded 2D Map from Figure 1, color-coded ROIs, and SUV_{BW} values is depicted. The four color wheels on the right show ROI color-codings for varying N s. For the report, the upmost color wheel with $N = 9$ was employed and the respective values are listed in Table 1.

To evaluate the accuracy of Algorithm 1, resulting SUV_{BW} values were compared to SUVs that were obtained using the VG51C software (cf. Fig. 2). This was done by manually reconstructing ROI segmentations from exported screenshots. Regarding $SUV_{max;BW}$ values, for each ROI, there were no differences and thus, the presented algorithm produces reliable and reproducible results. However, this was not the case for $SUV_{\mu;BW}$ values, since even small differences between ROIs can result in significantly different SUVs, which can influence diagnosis and therapy decisions [5].

Currently, the proposed map-based approach only depicts diagnoses with respect to the N-staging component for thoracic lymph nodes [10]. However, the basic idea behind the presented approach can be extended to cover the tumor and metastasis components of the TNM staging system, or to cover other organs, e. g., the liver or prostate. One shortcoming of the visualization-supported reports is that color printers are required, which have higher running costs compared to monochrome printers, but the enhanced reports have the potential to be better understood by a broader clinical audience.

5 Conclusion

We presented how clinical reports can be supported via standardized map-based visualizations. Two color-coding methods were presented. The first method can be used for map-based depictions of LNSs and anatomical landmarks, and the second method can be applied to color-code an arbitrary number of ROI segmentations in PET image data. The second method defines colors in a hue range that can be adjusted to not visually overlap with PET image color-codings to decrease the risk of misinterpretations. Finally, a guide was presented to compute reproducible SUV_{BW} values. Where applicable, methods were compared to a clinical toolbox.

Acknowledgements This work is partly funded by the Federal Ministry of Education and Research within the Forschungscampus *STIMULATE* (Grant Number 13GW0095A).

Supplementary Material The colored version can be found at <http://www.vismd.de>

References

- [1] Birr, S., Dicken, V., et al., *3D-PDF: Ein interaktives Tool für das onkologische Reporting und die Operationsplanung von Lungentumoren*, In: Proc. of German Society of Computer- and Robot-Assisted Surgery (CURAC), Magdeburg, Germany, Sept. (2011)
- [2] Brewer, C. A., *Color Use Guidelines for Mapping and Visualization*, Vis Mod Cartogr, **2**, pp. 123–148 (1994)
- [3] Foster, B., Bagci, U., et al., *A Review on Segmentation of Positron Emission Tomography Images*, Comput Biol Med, **50**, pp. 76–96 (2014)
- [4] Itten, J., *The Art of Color*, ISBN: 0471289280, New York, USA (1973)
- [5] Joo Hyun, O., Lodge, M. A., et al., *Practical PERCIST: A Simplified Guide to PET Response Criteria in Solid Tumors 1.0*, Radiology, **280**(2), 576–584 (2016)
- [6] Klein, J. L., Garcia, E. V., et al., *Reversibility Bull’s-Eye*, J Nucl Med, **31**(7), pp. 1240–1246 (1990)
- [7] Kreiser, J., Meuschke, M., et al., *A Survey of Flattening-Based Medical Visualization Techniques*, In: Computer Graphics Forum (CGF) (2018)
- [8] Merten, N., Genseke, P., et al., *Towards Automated Reporting and Visualization of Lymph Node Metastases of Lung Cancer*, In: Proc. of Workshop Bildverarbeitung für die Medizin (BVM), Lübeck, Germany, Mar. (2019)
- [9] Mountain, C. F., Dresler, C. M., *Regional Lymph Node Classification for Lung Cancer Staging*, Chest, **111**(6), pp. 1718–1723 (1997)
- [10] Rami-Porta, R., Crowley, J. J., et al., *The Revised TNM Staging System for Lung Cancer*, Ann Thorac Cardiovas, **15**(1), pp. 4–9 (2009)
- [11] Reiner, B., Siegel, E., *Radiology Reporting: Returning to Our Image-Centric Roots*, Am J Roentgenol, **187**(5), pp. 1151–1155 (2006)
- [12] Ritter, F., Boskamp, T., et al., *Medical Image Analysis*, IEEE Pulse, **2**(6), pp. 60–70 (2011)
- [13] Rössling, I., Dornheim, J., et al., *The Tumor Therapy Manager*, In: Proc. of Information Processing in Computer-Assisted Interventions (IPCAI), Berlin, Germany, June (2011)
- [14] Soongsathitanon, S., Masa-Ah, P., et al., *A new Standard Uptake Values (SUV) Calculation Based on Pixel Intensity Values*, Int J Math Comput Simul, **50**(1), pp. 26–33 (2012)
- [15] Tufte, E. R., *The Visual Display of Quantitative Information*, ISBN: 0961392142, Cheshire, CT, USA (2001)